Generation of Ultrabrilliant Polarized Attosecond Electron Bunches via Dual-Wake Injection

Ting Sun,[1] Qian Zhao[ORCID],[1,*] Feng Wan,[1] Yousef I. Salamin[ORCID],[2] and Jian-Xing Li[1,3,†]

[1]*Ministry of Education Key Laboratory for Nonequilibrium Synthesis and Modulation of Condensed Matter,
Shaanxi Province Key Laboratory of Quantum Information and Quantum Optoelectronic Devices, School of Physics,
Xi'an Jiaotong University, Xi'an 710049, China*
[2]*Department of Physics, American University of Sharjah, Sharjah, POB 26666 Sharjah, United Arab Emirates*
[3]*Department of Nuclear Physics, China Institute of Atomic Energy, P.O. Box 275(7), Beijing 102413, China*

Laser wakefield acceleration is paving the way for the next generation of electron accelerators, for their own sake and as radiation sources. A controllable dual-wake injection scheme is put forward here to generate an ultrashort triplet electron bunch with high brightness and high polarization, employing a radially polarized laser as a driver. We find that the dual wakes can be driven by both transverse and longitudinal components of the laser field in the quasiblowout regime, sustaining the laser-modulated wakefield which facilitates the subcycle and transversely split injection of the triplet bunch. Polarization of the triplet bunch can be highly preserved due to the laser-assisted collective spin precession and the noncanceled transverse spins. In our three-dimensional particle-in-cell simulations, the triplet electron bunch, with duration about 500 as, six-dimensional brightness exceeding 10^{14} A/m^2/0.1% and polarization over 80%, can be generated using a few-terawatt laser. Such an electron bunch could play an essential role in many applications, such as ultrafast imaging, nuclear structure and high-energy physics studies, and the operation of coherent radiation sources.

Laser wakefield acceleration (LWFA), especially in the blowout regime driven by an intense laser pulse, can accelerate electrons within the focusing and accelerating phases of a plasma wave (essentially in one quarter of a plasma wavelength) and can generate high-brightness femtosecond electron bunches [1–5]. Quality of the wakefield electron bunch is strongly injection-scheme dependent, and the controllable schemes include field-ionization injection [6–9], density-gradient injection [10,11], and magnetic-field controlled injection [12,13]. Highly localized injection can be implemented in order to accelerate ultrashort electron bunches even at the attosecond scale in LWFA [14–17]. A femtosecond (or attosecond) electron bunch with very high brightness underpins ultrafast imaging and microscopy [18–22] and can be used as an injection beam in a multistage wakefield acceleration setup to achieve high-quality GeV particle energies [23,24]. Six-dimensional (6D) brightness, which characterizes the high-quality wakefield electron bunch [25], can reach about 10^{15} A/m^2/0.1% in experiments [26], and is utilized in the operation of a free electron laser for injection [27–30], and in the generation of compact monoenergetic sources of γ rays and coherent x rays [31–34]. It has also been recently proposed that the polarized electrons can be generated in a controllable LWFA scheme [35–40], in which a prepolarized gas target can be prepared experimentally, with densities reaching 10^{19}–10^{20} cm^{-3}, via ultraviolet

photodissociation of a hydrogen-halogen molecule [41–44]. The polarization can enhance the capacity of a high-brightness electron bunch for utilization in a range of applications [45], such as investigating the properties of a magnetic material [46], nuclear structure studies [47,48], and the construction of polarized γ-ray sources [33,49,50].

For production of a highly polarized electron bunch in the plasma wakefield, depolarization must be mitigated. The characteristic depolarization in a wakefield originates predominantly from the sheath-current-induced azimuthal magnetic field during injection [36,40]. Specifically, depolarization results from two sources: (i) continuous injection of the electrons induces disperse precessions of initial spins due to the evolving wakefield, and (ii) the azimuthally symmetric distribution of transverse spins results in cancellation. Although depolarization from source (i) can be mitigated by fine control of the driver and plasma parameters for the moderately relativistic intensity of wakefield, the attainable current intensity and brightness are significantly limited [36–39,51]. Because of the azimuthal symmetry of the sheath current, depolarization from source (ii) cannot be eliminated in the currently available injection schemes, to the best of our knowledge. In principle, spin precession of the sheath electrons in the blowout regime can be synchronized via ultrashort injection, even at the attosecond scale, which results in the collective spin rotation of an electron bunch, thus circumventing
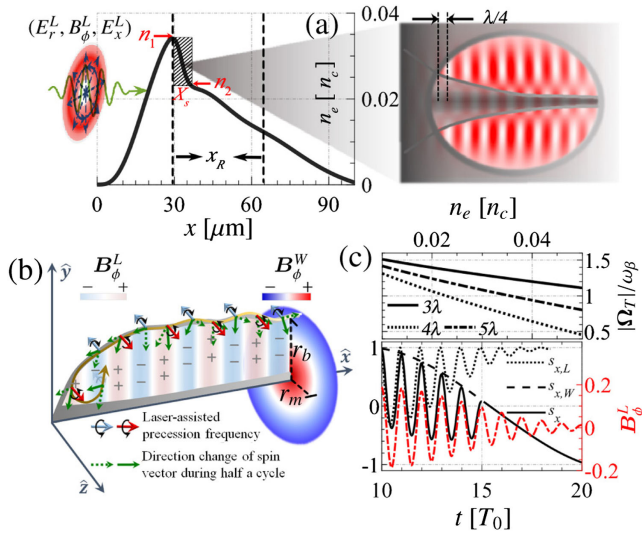
FIG. 1. (a) Plasma density profile with a transition length X_s between n_1 and n_2, with the Rayleigh length x_R of a RPL pulse also labeled. The schematic dual-wake plasma bubble is overlapped by the analytical laser intensity $(E_x^L)^2 + (E_r^L)^2$ used in the simulations. (b) Sketch of the spin precession of an electron inside a plasma bubble. (c) Top: ratio of spin precision frequency Ω_T and betatron frequency ω_β vs n_e, for different laser spot sizes. Bottom: spin precession vs time in laser field ($s_{x,L}$), wakefield ($s_{x,W}$), and superposed field (s_x).

depolarization from source (i). Nevertheless, the currently available methods of attosecond injection in the blowout regime still cause depolarization from source (ii) [14–17]. Still, generation of a high-brightness polarized electron bunch remains challenging.

In this Letter, we put forward a dual-wake injection scheme for LWFA, as a result of which an ultrashort electron bunch with high brightness and high polarization can be generated. In this scheme, a tightly focused radially polarized laser (RPL) pulse propagates through a plasma with the density profile of a near-critical-density peak and a sharp downward density jump, driving dual wakes in the quasiblowout wake (QBW) regime [52]; see Fig. 1(a). The laser-modulated wakefield in the dual wakes induces oscillatory spin precession of the sheath electrons, whereby the initial spin directions can be reversed at the end of the injection stage; see Fig. 1(b). The principal parameters of laser and plasma density, modeling the laser-assisted spin precession, are elucidated analytically; see Fig. 1(c). Three-dimensional (3D) particle-in-cell (PIC) simulations indicate that the driven dual wakes cause the subcycle injection of the transversely split triplet bunch, and demonstrate that the depolarization is significantly mitigated due to the approximately collective spin precession and transverse spins that survive cancellation; see Figs. 2 and 3. The dynamical processes associated with the spin precessions are elucidated by carefully tracking the trajectories of individual electrons in one beam of the triplet bunch; see Fig. 4. Robust generation of ultrashort electron bunches with high brightness and high polarization is tested by varying the transition length of density jump; see Fig. 5.

The blowout regime arises when the laser pulse duration τ_L matches the plasma wave period, i.e., when $c\tau_L \lesssim 2\sqrt{a_0}/k_p$ [5]. Here, $k_p = \omega_p/c$, with the plasma frequency ω_p and the speed of light in vacuum c, and a_0 is amplitude of the laser vector potential. Violation of this condition for a relatively long τ_L results in the QBW regime in which the laser pulse overlaps the wake bucket. A tightly focused RPL pulse has an intense longitudinal electric field E_x^L, a radial electric field E_r^L and an azimuthal magnetic field B_ϕ^L [53,54], resembling the configuration of the plasma wake-field and, thus, can be used to excite the laser-modulated wakefield in the QBW regime. For a strongly nonlinear plasma wake, the betatron frequency, $\omega_\beta = \omega_p/\sqrt{2\gamma_e}$, with $\gamma_e \simeq \sqrt{1 + a_0^2/2}$ in the ponderomotive approximation, characterizes the formation time of a plasma bubble by half the betatron period $\tau_\beta = 2\pi/\omega_\beta$ [55]. A RPL pulse of wavelength $\lambda = 0.8$ μm, power 10 TW, pulse duration $5T_0$ and a spot size of $w_0 = 4\lambda$, has $\tau_\beta/2$ in the range $\simeq 8T_0$ to $5T_0$, which corresponds to a density range of $n_e = 0.02n_c$ to $0.05n_c$. Here, $T_0 = \lambda/c$, and n_c is the critical density.

In a feasible setup, the plasma density profile can be initialized with a near-critical density peak and a sharp downward density jump to realize the controllable injection of high-quality electron bunches, which can be prepared experimentally by triggering a shock front in a supersonic gas jet [56–58]. This density profile can be modeled by an analytical function with the combination of a Γ distribution function and an asymmetric double sigmoidal function [59], where the density jump can be characterized by the transition length X_s and the density ratio n_2/n_1 and parametrized according to the kinetic theory of gases [60]; see left panel of Fig. 1(a). Thus, under the conditions of the QBW regime and tight focusing of RPL pulse, the dual wakes can be driven in this density profile with a E_r^L-driven donut wake and a E_x^L-driven nonclosed wake; see right panel of Fig. 1(a). The sheath electrons ride on the laser phases in the injection region of the dual wakes and get modulated by both the longitudinal and transverse laser fields, with a $\lambda/4$ overlap. The longitudinal trapping condition in the RPL-driven QBW is modified due to the superposed laser vector potential and described by variation of the pseudopotential $\Delta\psi \leq \sqrt{1 + \beta_\perp^2}/\gamma_b - 1 + \Delta\psi^L$, where $\Delta\psi^L = ev_b/m_ec^2[A_x^L(r_f) - A_x^L(r_i)]$, in which $E_x^L = -\partial A_x^L/\partial t$, and r_i and r_f, respectively, are the initial and final radial positions of a sheath electron [13]. Here, m_e and e are the electron mass and charge, respectively. A sheath electron should be injected into the acceleration phase of E_x^L in order for it to copropagate with the laser, which implies that the sheath electrons experience integer numbers of laser cycles between $A_x^L(r_f)$ and $A_x^L(r_i)$, and undergo subcycle injection.
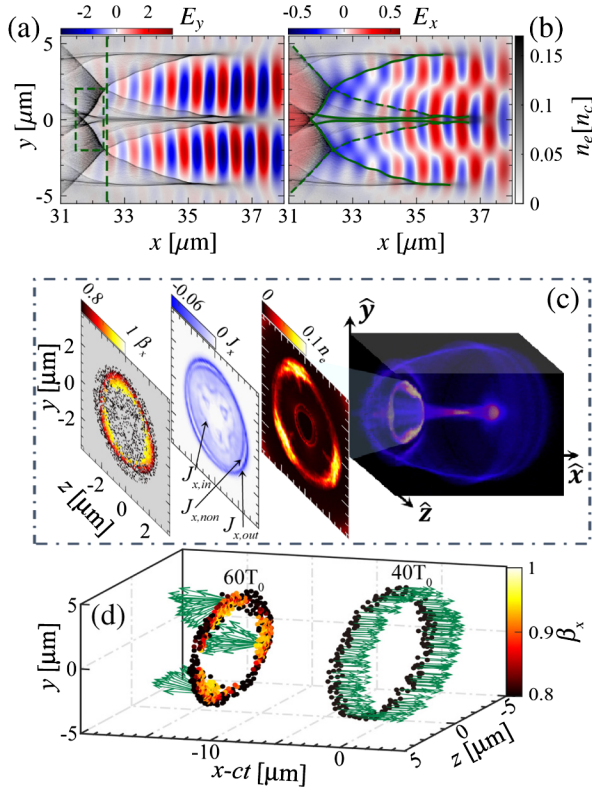
FIG. 2. Snapshot at a propagation time $t = 52T_0$ of the plasma density n_e (gray) with (a) the transverse electric fields E_y and (b) the longitudinal electric field E_x, superimposed upon it. The injection region is indicated within a dashed rectangle and structure of the wakes is indicated by solid and dashed lines. (c) 3D plasma density with the projection of injected electrons on the y–z plane. Transverse distributions of normalized current density J_x and longitudinal velocity β_x are sliced at the dash-lined position of (a). (d) Sheath electrons with the spin directions (green arrows) before and after injection.
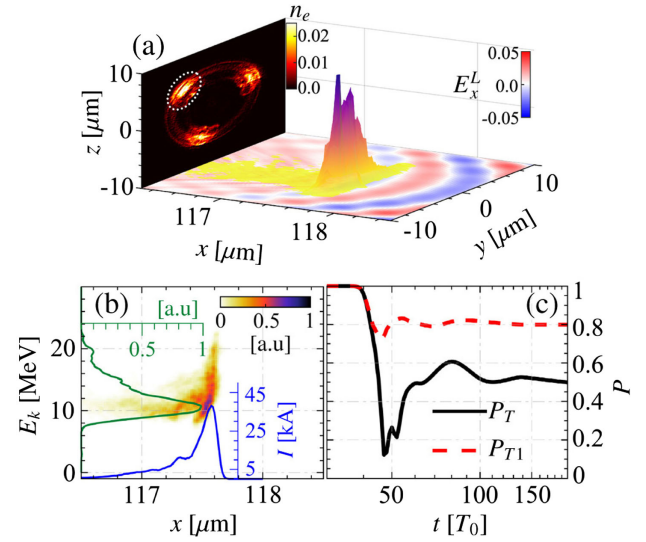

FIG. 3. (a) Transverse and longitudinal density distributions of injected electron bunches at a propagation time $t = 160T_0$, and the laser's longitudinal electric field E_x^L is mapped on the propagation plane. (b) Phase-space distribution of one beam of the triplet bunch [shown inside a dotted ellipse in (a)] with the energy spectrum and current distribution. (c) Temporal evolution of polarization for the triplet bunch (P_T) and one of its component beams (P_{T1}).

In what follows, $a_l = \omega/\omega_p$, unless explicitly stated, and the electric and magnetic fields are normalized by $e/(m_e c\omega)$ and $e/(m_e\omega)$, respectively, with ω the laser frequency. By analogy to the donut wake driven by a Laguerre-Gaussian laser [61], components of the spherical bubble field are $E_r^W = k_p(r - r_m)/4a_l$, $B_\phi^W = -k_p(r - r_m)/4a_l$, and $E_x^W = k_p(x - r_b - v_b t)/2a_l$, where $r_m \simeq w_0/\sqrt{2}$, $r_b \simeq 2\sqrt{a_\perp}$, with a transverse laser vector potential $a_\perp$ and a bubble velocity v_b. For a bubble sheath electron with spin vector $\mathbf{s} = (s_r, s_\phi, s_x)$ in cylindrical coordinates, irrespective of the Sokolov-Ternov effect ($\sim$ms scale in our model) [59] and the negligible Stern-Gerlach force in LWFA [62], the spin precession can be described by the Thomas-Bargmann-Michel-Telegdi (TBMT) equation [63] $d\mathbf{s}/dt = \mathbf{\Omega} \times \mathbf{s} = (\mathbf{\Omega}_T + \mathbf{\Omega}_a) \times \mathbf{s}$, where $\mathbf{\Omega}_a = a[\mathbf{B} - (\gamma_e/\gamma_e + 1)\boldsymbol{\beta}(\boldsymbol{\beta} \times \mathbf{B}) - \boldsymbol{\beta} \times \mathbf{E}]$, with the anomalous magnetic moment of the electron $a \approx 1.16 \times 10^{-3}$, and $\mathbf{\Omega}_T = (\mathbf{B}/\gamma_e) - (1/(\gamma_e + 1))\boldsymbol{\beta} \times \mathbf{E}$. Recall that $|\mathbf{\Omega}_a| \ll |\mathbf{\Omega}_T|$, $\mathbf{\Omega}_T^I \simeq B_\phi^W \hat{\boldsymbol{\phi}}/\gamma_e$ dominates the spin

precession of a wakefield electron during the injection stage, and $\mathbf{\Omega}_T^{II} \simeq (B_\phi^W - E_r^W)\hat{\boldsymbol{\phi}}/\gamma_e = -F_{W,\perp}\hat{\boldsymbol{\phi}}/\gamma_e$ dominates during the acceleration stage [35,36,40]. In the laser-modulated wakefield, the spin precession of a sheath electron is also influenced by B_ϕ^L and displays oscillatory precession in each optical cycle. Qualitatively, B_ϕ^W causes the net precession and B_ϕ^L causes the change of precession direction at the end of the injection stage, resulting in the laser-assisted spin precession of a sheath electron and reversal of the spin vector; see in Fig. 1(b).

The laser-assisted spin precession can be elucidated by resorting to the TBMT equation, using the spherical bubble fields. Variation of the ratio $|\mathbf{\Omega}_T|/\omega_\beta$ with the plasma density, for different values of w_0, is shown in Fig. 1(c), top. Note that $|\mathbf{\Omega}_T|$ can be comparable to the betatron frequency ω_β in the bubble wakefield. The critical $|\mathbf{\Omega}_T|/\omega_\beta = 1$ means that the spin precession and betatron oscillation are synchronous, causing $\mathbf{s}$ to reverse direction as a sheath electron slips back to the bottom of the bubble, and the depolarization increases linearly with density. To distinguish this from the case of the wakefield [35,36,40], the laser-assisted precession frequencies are denoted by $\mathbf{\Omega}_T^{\prime I} \simeq (B_\phi^L + B_\phi^W)\hat{\boldsymbol{\phi}}/\gamma_e$ and $\mathbf{\Omega}_T^{\prime II} \simeq (F_{W,\perp} + F_{L,\perp})\hat{\boldsymbol{\phi}}/\gamma_e$, corresponding to the injection and acceleration stages, respectively, of the laser-modulated wakefield, with $F_{L,\perp} = E_r^L - B_\phi^L$ resulting from employing the RPL fields beyond the paraxial approximation. Calculations, employing $s_x = \cos(|\mathbf{\Omega}_T^{\prime I}|\tau_\beta/2)$, indicate that the net precession,

from $s_x = 1$ to $s_x \simeq 0$ at $15T_0$, may be obtained from $\boldsymbol{B}_\phi^W$, whereas the upward precession direction (from $s_x = -1$ to $s_x = 1$ and vice versa) is due to the focused phase of $\boldsymbol{B}_\phi^L$; see Fig. 1(c), bottom. After $t = 15T_0$, s_x precesses at $\boldsymbol{\Omega}_T^{II}$ with a downward precession direction due to the laser-phase-locked injection into the defocused field with negative $F_{L,\perp} + F_{W,\perp}$.

In order to visualize the polarized acceleration in the dual-wake injection scheme, 3D PIC simulations have been carried out using EPOCH and incorporating the TBMT equations [64,65]. In each case, a moving window along the x direction is used, with a $25\lambda(x) \times 25\lambda(y) \times 25\lambda(z)$ simulation box divided into $640 \times 160 \times 160$ cells. The explicit truncated series expressions modeling the fields of a focused RPL pulse are used [53], initialized with 10 TW power, $w_0 = 3$ μm and $\tau_L = 10$ fs. With $X_s = 6$ μm and $n_2/n_1 = 0.66$, the dual wakes sustaining the laser-modulated wakefield are driven near the focal plane (at $x = 30$ μm); see Figs. 2(a) and 2(b). $F_{L,\perp}$ drives the donut wake bucket (solid lines) with closed outer-sheath density and almost merged inner-sheath density, and the intense E_x^L sweeps over the inner-sheath density and drives the outward nonclosed sheath density (solid-dashed lines) due to the near-axis defocusing field [59]. The annular sheath electrons are accelerated and split into the Clover-like distribution transversely due to the transversely structured current density; see Fig. 2(c). The inner-sheath current $J_{x,\text{in}}$ senses the transversely nonuniform longitudinal field E_x at the bottom of the donut wake [Fig. 2(b)], leading to the deformed transverse distribution of the nonclosed sheath current $J_{x,\text{non}}$. The current $J_{x,\text{non}}$ intersects with the outer-sheath current $J_{x,\text{out}}$, which weakens J_x in the crossing sectors. As a result, pseudopotential ψ of the wakefield exhibits transverse asymmetry, according to Poisson's equation $-\nabla_\perp^2 \psi = (\rho - J_x)$, with a transversely structured current source J_x, which gives rise to (the transversely asymmetric) E_x^W [2,59]. Consequently, the Clover-like sheath electrons are injected with the subcycle duration and transversely split beams, which constitutes the "dual-wake injection." Furthermore, because of the approximate match between ω_β and Ω_T^{II}, spins of the injected electrons possess a collective precession orientation toward $s_x = -1$; see Fig. 2(d). Statistical polarization of the electrons is $P = \sqrt{\bar{s}_x^2 + \bar{s}_y^2 + \bar{s}_z^2}$, with $\bar{s}_{x,y,z}$ the components averaged over the particle number.

The injected Clover-like sheath electrons undergo direct laser acceleration by E_x^L and get transversely modulated into the three beams making up the "triplet bunch"; see Fig. 3(a). Because of the laser spot defocusing beyond the focal plane, an opening angle $\delta\theta \simeq 0.135$ rad is associated with the triplet bunch, leading to the completely isolated beams of that bunch (see details in Fig. 7 of [59]). The corresponding phase-space distribution of one beam of the triplet bunch is shown in Fig. 3(b). The quasimonoenergetic
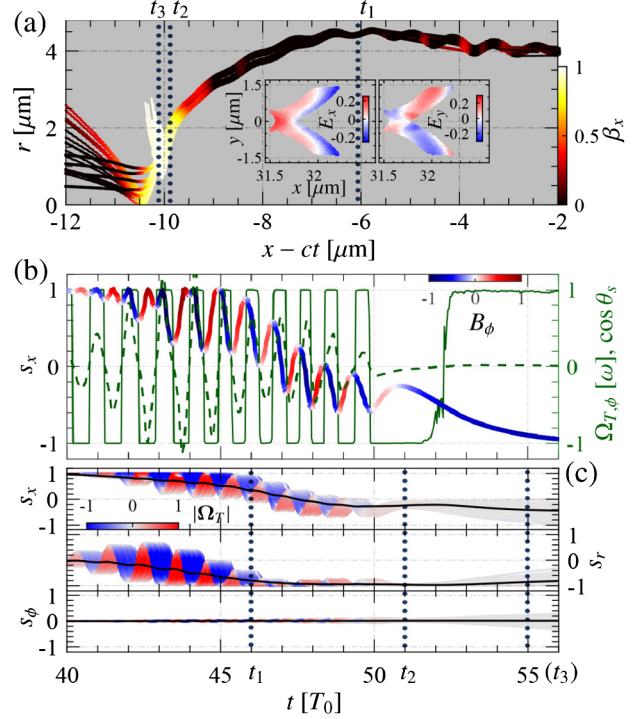

FIG. 4. (a) Trajectories of the randomly selected sheath electrons from the injection region in Fig. 2(a), color coded by the longitudinal velocities. Insets: Snapshot of the tracked electrons at $52T_0$, color coded by the sensed longitudinal and transverse fields. (b) Left axis: precession of s_x of an injected electron color coded by its transient magnetic field B_ϕ. Right axis: temporal evolution of $\cos\theta_s$ (green-solid line) and $\Omega_{T,\phi}$ (green-dashed line). (c) Precession of the spin components of electrons in one beam of the triplet bunch, color coded by the transient precession frequency. The averaged spin components are represented by black-solid lines.

attosecond bunch has a pulse duration of $\sim T_0/4$, a normalized transverse emittance of $\varepsilon_{n,y(z)} \simeq 0.02(0.03)$ mm mrad, and a peak current of ~ 38 kA. Evolution of polarization of the triplet bunch is distinguished from that of one of its component beams; see Fig. 3(c). P_T comes essentially from the averaged longitudinal spin component $\bar{s}_x$, due to cancellation of the transverse spin component s_r. P_T drops to zero, followed by a one-period oscillation, before rising to the final stable 50%, during which spin vectors of the injected electrons successively undergo full reversal within a time of about $\tau_\beta/2$; as explained in the caption of Fig. 4. On the other hand, P_{T1} is highly preserved during the entire evolution, due to the approximately collective precession with the nonvanishing polarization from s_r.

The subcycle injection and laser-assisted spin precession in the laser-modulated wakefield can both be clarified by tracking the trajectories of sheath electrons. The fields sensed by the electrons in the injection region exhibit overlap of $\lambda/2$ focusing phase and $\lambda/4$ acceleration phase; see the insets of Fig. 4(a). The corresponding trajectories
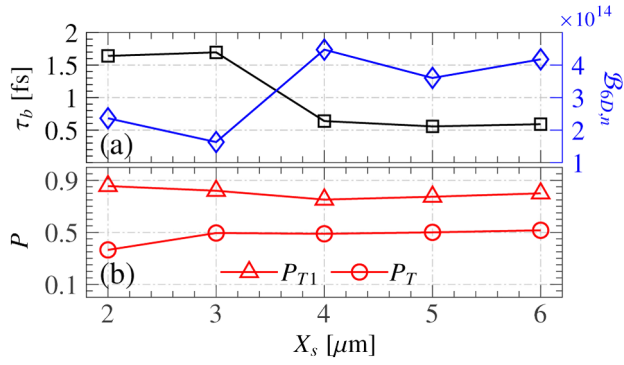
FIG. 5.   (a) Root-mean-square bunch duration τ_b and 6D brightness $\mathcal{B}_{6D,n}$ of one beam of the triplet bunch vs the scale length X_s of the density jump. (b) Variations of P_T and P_{T1} with X_s.

indicate that the sheath electrons slip to the center of the wake bucket at t_1, and the injection occurs between t_2 and t_3. During the injection, only the sheath electrons located by laser acceleration phase are injected and get modulated into an attosecond bunch with $\sim T_0/4$ duration; see trajectories after t_3 in Fig. 4(a). The injected electrons maintain polarization during the injection stage. The direction of $\mathbf{\Omega}_T(t)$ will be expressed in terms of $\cos\theta_s$, where θ_s is the angle it makes with the initial $\mathbf{\Omega}_T(t_0)$. In addition, $|\mathbf{\Omega}_T|$ approximately equals its azimuthal component $\Omega_{T,\phi}$ by recalling the azimuthal vectors $\mathbf{\Omega}_T'^I$ and $\mathbf{\Omega}_T'^{II}$ (see details in Fig. 4 of [59]). Temporal evolution of the spin-precession frequency, shown in Fig. 4(b), has been obtained from investigating the dynamics of a randomly chosen electron in the triplet bunch. The square-wave-like variation of $\cos\theta_s$ is consistent with the oscillating $\Omega_{T,\phi}$, which confirms the azimuthal nature of $\mathbf{\Omega}_T$. Beginning with the symmetric oscillation before t_1, $\Omega_{T,\phi}$ exhibits asymmetric oscillations between t_1 and t_2, due to the rising wakefield B_ϕ^W, which leads to the net precession from $s_x = 1$ to $s_x \simeq 0$ within $5T_0$. As explained, in principle, in Fig. 1(c), the precession direction of the electron is upward before t_2 and is reversed again towards $s_x = -1$ after the injection, resulting in high polarization. Because of the similar $|\mathbf{\Omega}_T|$ for each electron during the injection stage, s_x and s_r of them possess almost the same precession before t_2, which leads to the collective rotation of spin vectors and the nondeteriorating P_{T1}; see Fig. 4(c). Planar motion of the sheath electrons indicates that there is almost no precession along the azimuthal direction before injection, while the precession of s_ϕ occurs during laser modulation of the electrons after injection.

Robustness of the dual-wake injection scheme can be examined by changing parameters of the sharp downward density jump. With the theoretical estimates (see details in Fig. 5 of [59]), X_s and n_2/n_1 can, respectively, be approximated as (2, 3, 4, 5, 6) μm, and (0.4, 0.51, 0.56, 0.6, 0.66), for the sake of parametrizing the density profile in Fig. 1(a). For values of X_s smaller than the plasma

wavelength λ_{p1} ($\simeq$4.3 μm at n_1), the shock-front injection, which leads to injection of the density peak of the wake bucket driven at n_1 into the adjacent wake bucket driven at n_2 [57], leads to the injected bunch with length of $\sim\lambda/2$. As X_s increases beyond λ_{p1}, the relatively gentle density gradient generates the attosecond bunch of length $\lambda/4$; see Fig. 5(a). The 6D brightness $\mathcal{B}_{6D,n}$ increases up to $\sim 4 \times 10^{14}$ A/m^2/0.1% as $X_s > 3$ μm where the density-gradient injection leads to the narrower energy spectra [59]. This is close to the maximum $\sim 10^{15}$ A/m^2/0.1%, obtained by state-of-the-art LWFA and linac bunches [25,26]. P_T and P_{T1} are almost independent of X_s, because spin precession of the sheath electrons mainly occurs during the wake formation time $\tau_\beta/2$, which undergoes minor changes due to slight variations in X_s; see Fig. 5(b).

With currently available laser technology, a femtosecond RPL pulse with peak power exceeding 85 GW is attainable in experiments [66,67]. Terawatt-power beams seem feasible via the technology of optical parametric amplification [68]. So, the potential exists for such a system to be used to experimentally realize our dual-wake injection scheme in a RPL-driven QBW regime.

In conclusion, generation of the ultrashort triplet electron bunch with high brightness and high polarization has been investigated in the dual-wake injection scheme for LWFA. In this scheme, the laser-modulated wakefield in a donut QBW leads to the subcycle and the transversely split injection of the triplet electron bunch. High polarization of the triplet electron bunch can be preserved due to the laser-assisted spin precession and noncanceled transverse spins. Our 3D PIC simulations demonstrate robust generation of the ultrashort electron bunches with brightness over 10^{14} A/m^2/0.1% and polarization exceeding 80%. Such an electron bunch is advantageous as a source of polarized γ-rays and in applications in ultrafast imaging, nuclear physics and high-energy physics studies.

*zhaoq2019@xjtu.edu.cn
†jianxing@xjtu.edu.cn

[1] T. Tajima and J. M. Dawson, Laser electron accelerator, Phys. Rev. Lett. **43**, 267 (1979).

[2] W. Lu, C. Huang, M. Zhou, W. B. Mori, and T. Katsouleas, Nonlinear theory for relativistic plasma wakefields in the blowout regime, Phys. Rev. Lett. **96**, 165002 (2006).

[3] J. Faure, C. Rechatin, A. Norlin, A. Lifschitz, Y. Glinec, and V. Malka, Controlled injection and acceleration of electrons in plasma wakefields by colliding laser pulses, Nature (London) **444**, 737 (2006).

[4] O. Lundh, J. Lim, C. Rechatin, L. Ammoura, A. Ben-Ismail, X. Davoine, G. Gallot, J.-P. Goddet, E. Lefebvre, V. Malka, and J. Faure, Few femtosecond, few kiloampere electron bunch produced by a laser-plasma accelerator, Nat. Phys. **7**, 219 (2011).

[5] E. Esarey, C. B. Schroeder, and W. P. Leemans, Physics of laser-driven plasma-based electron accelerators, Rev. Mod. Phys. **81**, 1229 (2009).

[6] M. Chen, Z. M. Sheng, Y. Y. Ma, and J. Zhang, Electron injection and trapping in a laser wakefield by field ionization to high-charge states of gases, J. Appl. Phys. **99**, 056109 (2006).

[7] A. Pak, K. A. Marsh, S. F. Martins, W. Lu, W. B. Mori, and C. Joshi, Injection and trapping of tunnel-ionized electrons into laser-produced wakes, Phys. Rev. Lett. **104**, 025003 (2010).

[8] C. McGuffey, A. G. R. Thomas, W. Schumaker, T. Matsuoka, V. Chvykov, F. J. Dollar, G. Kalintchenko, V. Yanovsky, A. Maksimchuk, K. Krushelnick, V. Y. Bychenkov, I. V. Glazyrin, and A. V. Karpeev, Ionization induced trapping in a laser wakefield accelerator, Phys. Rev. Lett. **104**, 025004 (2010).

[9] M. Chen, E. Esarey, C. B. Schroeder, C. G. R. Geddes, and W. P. Leemans, Theory of ionization-induced trapping in laser-plasma accelerators, Phys. Plasmas **19**, 033101 (2012).

[10] C. G. R. Geddes, K. Nakamura, G. R. Plateau, C. Toth, E. Cormier-Michel, E. Esarey, C. B. Schroeder, J. R. Cary, and W. P. Leemans, Plasma-density-gradient injection of low absolute-momentum-spread electron bunches, Phys. Rev. Lett. **100**, 215004 (2008).

[11] A. J. Gonsalves, K. Nakamura, C. Lin, D. Panasenko, S. Shiraishi, T. Sokollik, C. Benedetti, C. B. Schroeder, C. G. R. Geddes, J. van Tilborg, J. Osterhoff, E. Esarey, C. Toth, and W. P. Leemans, Tunable laser plasma accelerator based on longitudinal density tailoring, Nat. Phys. **7**, 862 (2011).

[12] J. Vieira, S. F. Martins, V. B. Pathak, R. A. Fonseca, W. B. Mori, and L. O. Silva, Magnetic control of particle injection in plasma based accelerators, Phys. Rev. Lett. **106**, 225001 (2011).

[13] Q. Zhao, S. M. Weng, Z. M. Sheng, M. Chen, G. B. Zhang, W. B. Mori, B. Hidding, D. A. Jaroszynski, and J. Zhang, Ionization injection in a laser wakefield accelerator subject to a transverse magnetic field, New J. Phys. **20**, 063031 (2018).

[14] M. J. H. Luttikhof, A. G. Khachatryan, F. A. van Goor, and K.-J. Boller, Generating ultrarelativistic attosecond electron bunches with laser wakefield accelerators, Phys. Rev. Lett. **105**, 124801 (2010).

[15] M. P. Tooley, B. Ersfeld, S. R. Yoffe, A. Noble, E. Brunetti, Z. M. Sheng, M. R. Islam, and D. A. Jaroszynski, Towards attosecond high-energy electron bunches: Controlling self-injection in laser-wakefield accelerators through plasma-density modulation, Phys. Rev. Lett. **119**, 044801 (2017).

[16] Q. Zhao, S. Weng, M. Chen, M. Zeng, B. Hidding, D. Jaroszynski, R. Assmann, and Z. Sheng, Sub-femtosecond electron bunches in laser wakefield acceleration via injection suppression with a magnetic field, Plasma Phys. Controlled Fusion **61**, 085015 (2019).

[17] J. Kim, T. Wang, V. Khudik, and G. Shvets, Subfemtosecond wakefield injector and accelerator based on an undulating plasma bubble controlled by a laser phase, Phys. Rev. Lett. **127**, 164801 (2021).

[18] P. Baum and A. H. Zewail, Attosecond electron pulses for 4D diffraction and microscopy, Proc. Natl. Acad. Sci. U.S.A. **104**, 18409 (2007).

[19] F. Krausz and M. Ivanov, Attosecond physics, Rev. Mod. Phys. **81**, 163 (2009).

[20] S. Corde, K. Ta Phuoc, G. Lambert, R. Fitour, V. Malka, A. Rousse, A. Beck, and E. Lefebvre, Femtosecond x rays from laser-plasma accelerators, Rev. Mod. Phys. **85**, 1 (2013).

[21] R. J. D. Miller, Femtosecond crystallography with ultrabright electrons and x-rays: Capturing chemistry in action, Science **343**, 1108 (2014).

[22] Y. Morimoto and P. Baum, Diffraction and microscopy with attosecond electron pulse trains, Nat. Phys. **14**, 252 (2018).

[23] J. Luo, M. Chen, W. Y. Wu, S. M. Weng, Z. M. Sheng, C. B. Schroeder, D. A. Jaroszynski, E. Esarey, W. P. Leemans, W. B. Mori, and J. Zhang, Multistage coupling of laserwakefield accelerators with curved plasma channels, Phys. Rev. Lett. **120**, 154801 (2018).

[24] X. Zhu, B. Li, F. Liu, J. Li, Z. Bi, X. Ge, H. Deng, Z. Zhang, P. Cui, L. Lu, W. Yan, X. Yuan, L. Chen, Q. Cao, Z. Liu, Z. Sheng, M. Chen, and J. Zhang, Experimental demonstration of laser guiding and wakefield acceleration in a curved plasma channel, Phys. Rev. Lett. **130**, 215001 (2023).

[25] S. Di Mitri and M. Cornacchia, Electron beam brightness in linac drivers for free-electron-lasers, Phys. Rep. **539**, 1 (2014).

[26] W. T. Wang, W. T. Li, J. S. Liu, Z. J. Zhang, R. Qi, C. H. Yu, J. Q. Liu, M. Fang, Z. Y. Qin, C. Wang, Y. Xu, F. X. Wu, Y. X. Leng, R. X. Li, and Z. Z. Xu, High-brightness highenergy electron beams from a laser wakefield accelerator via energy chirp control, Phys. Rev. Lett. **117**, 124801 (2016).

[27] Z. Huang, Y. Ding, and C. B. Schroeder, Compact x-ray free-electron laser from a laser-plasma accelerator using a transverse-gradient undulator, Phys. Rev. Lett. **109**, 204801 (2012).

[28] W. Wang, K. Feng, L. Ke, C. Yu, Y. Xu, R. Qi, Y. Chen, Z. Qin, Z. Zhang, M. Fang, J. Liu, K. Jiang, H. Wang, C. Wang, X. Yang, F. Wu, Y. Leng, J. Liu, R. Li, and Z. Xu, Free-electron lasing at 27 nanometres based on a laser wakefield accelerator, Nature (London) **595**, 516 (2021).

[29] R. Pompili *et al.*, Free-electron lasing with compact beam-driven plasma wakefield accelerator, Nature (London) **605**, 659 (2022).

[30] M. Labat *et al.*, Seeded free-electron laser driven by a compact laser plasma accelerator, Nat. Photonics **17**, 150 (2023).

[31] K. Ta Phuoc, S. Corde, C. Thaury, V. Malka, A. Tafzi, J. P. Goddet, R. C. Shah, S. Sebban, and A. Rousse, All-optical Compton gamma-ray source, Nat. Photonics **6**, 308 (2012).

[32] N. D. Powers, I. Ghebregziabher, G. Golovin, C. Liu, S. Chen, S. Banerjee, J. Zhang, and D. P. Umstadter,

Quasi-monoenergetic and tunable x-rays from a laser-driven Compton light source, Nat. Photonics 8, 28 (2014).

[33] Y. Ma, J. Hua, D. Liu, Y. He, T. Zhang, J. Chen, F. Yang, X. Ning, H. Zhang, Y. Du, and W. Lu, Compact polarized x-ray source based on all-optical inverse Compton scattering, Phys. Rev. Appl. 19, 014073 (2023).

[34] T. Brümmer, S. Bohlen, F. Grüner, J. Osterhoff, and K. Põder, Compact all-optical precision-tunable narrowband hard Compton x-ray source, Sci. Rep. 12, 16017 (2022).

[35] J. Vieira, C.-K. Huang, W. B. Mori, and L. O. Silva, Polarized beam conditioning in plasma based acceleration, Phys. Rev. Accel. Beams 14, 071303 (2011).

[36] M. Wen, M. Tamburini, and C. H. Keitel, Polarized laser-wakefield-accelerated kiloampere electron beams, Phys. Rev. Lett. 122, 214801 (2019).

[37] Y. Wu, L. Ji, X. Geng, Q. Yu, N. Wang, B. Feng, Z. Guo, W. Wang, C. Qin, X. Yan, L. Zhang, J. Thomas, A. Hützen, A. Pukhov, M. Büscher, B. Shen, and R. Li, Polarized electron acceleration in beam-driven plasma wakefield based on density down-ramp injection, Phys. Rev. E 100, 043202 (2019).

[38] Y. Wu, L. Ji, X. Geng, Q. Yu, N. Wang, B. Feng, Z. Guo, W. Wang, C. Qin, X. Yan, L. Zhang, J. Thomas, A. Hützen, M. Büscher, T. P. Rakitzis, A. Pukhov, B. Shen, and R. Li, Polarized electron-beam acceleration driven by vortex laser pulses, New J. Phys. 21, 073052 (2019).

[39] Z. Nie, F. Li, F. Morales, S. Patchkovskii, O. Smirnova, W. An, N. Nambu, D. Matteo, K. A. Marsh, F. Tsung, W. B. Mori, and C. Joshi, In Situ generation of high-energy spin-polarized electrons in a beam-driven plasma wakefield accelerator, Phys. Rev. Lett. 126, 054801 (2021).

[40] H. C. Fan, X. Y. Liu, X. F. Li, J. F. Qu, Q. Yu, Q. Kong, S. M. Weng, M. Chen, M. Büscher, P. Gibbon, S. Kawata, and Z. M. Sheng, Control of electron beam polarization in the bubble regime of laser-wakefield acceleration, New J. Phys. 24, 083047 (2022).

[41] T. P. Rakitzis, P. C. Samartzis, R. L. Toomes, T. N. Kitsopoulos, A. Brown, G. G. Balint-Kurti, O. S. Vasyutinskii, and J. A. Beswick, Spin-polarized hydrogen atoms from molecular photodissociation, Science 300, 1936 (2003).

[42] D. Sofikitis, L. Rubio-Lago, L. Bougas, A. J. Alexander, and T. P. Rakitzis, Laser detection of spin-polarized hydrogen from HCl and HBr photodissociation: Comparison of H- and halogen-atom polarizations, J. Chem. Phys. 129, 144302 (2008).

[43] D. Sofikitis, C. S. Kannis, G. K. Boulogiannis, and T. P. Rakitzis, Ultrahigh-density spin-polarized H and D observed via magnetization quantum beats, Phys. Rev. Lett. 121, 083001 (2018).

[44] A. K. Spiliotis, M. Xygkis, M. E. Koutrakis, D. Sofikitis, and T. P. Rakitzis, Depolarization of spin-polarized hydrogen via collisions with chlorine atoms at ultrahigh density, Chem. Phys. Impact 2, 100022 (2021).

[45] T. Sun, Q. Zhao, K. Xue, Z.-W. Lu, L.-L. Ji, F. Wan, Y. Wang, Y. I. Salamin, and J.-X. Li, Production of polarized particle beams via ultraintense laser pulses, Rev. Mod. Plasma Phys. 6, 38 (2022).

[46] T. J. Gay, Physics and technology of polarized electron scattering from atoms and molecules, in Advances in Atomic, Molecular, and Optical Physics Vol. 57, edited by E. Arimondo, P. R. Berman, and C. C. Lin (Elsevier Academic Press Inc, San Diego, 2009), pp. 157–247.

[47] K. Abe et al. (E143 Collaboration), Precision measurement of the deuteron spin structure function g_1^d, Phys. Rev. Lett. 75, 25 (1995).

[48] V. Y. Alexakhin, Y. Alexandrov, G. D. Alexeev, M. Alexeev, A. Amoroso, B. Badełek, F. Balestra, J. Ball, J. Barth, G. Baum et al., The deuteron spin-dependent structure function g_1^d and its first moment, Phys. Lett. B 647, 8 (2007).

[49] Y.-F. Li, R. Shaisultanov, Y.-Y. Chen, F. Wan, K. Z. Hatsagortsyan, C. H. Keitel, and J.-X. Li, Polarized ultra-short brilliant multi-GeV γ rays via single-shot laser-electron interaction, Phys. Rev. Lett. 124, 014801 (2020).

[50] Y. Wang, M. Ababekri, F. Wan, Q. Zhao, C. Lv, X.-G. Ren, Z.-F. Xu, Y.-T. Zhao, and J.-X. Li, Brilliant circularly polarized γ-ray sources via single-shot laser plasma inter-action, Opt. Lett. 47, 3355 (2022).

[51] I. Barth and O. Smirnova, Spin-polarized electrons produced by strong-field ionization, Phys. Rev. A 88, 013401 (2013).

[52] J. L. Shaw, N. Lemos, L. D. Amorim, N. Vafaei-Najafabadi, K. A. Marsh, F. S. Tsung, W. B. Mori, and C. Joshi, Role of direct laser acceleration of electrons in a laser wakefield accelerator with ionization injection, Phys. Rev. Lett. 118, 064801 (2017).

[53] Y. I. Salamin, Accurate fields of a radially polarized Gaussian laser beam, New J. Phys. 8, 133 (2006).

[54] C. Varin, S. Payeur, V. Marceau, S. Fourmaux, A. April, B. Schmidt, P.-L. Fortin, N. Thiré, T. Brabec, F. Légaré, J.-C. Kieffer, and M. Piché, Direct electron acceleration with radially polarized laser beams, Appl. Sci. 3, 70 (2013).

[55] G. D. Tsakiris, C. Gahn, and V. K. Tripathi, Laser induced electron acceleration in the presence of static electric and magnetic fields in a plasma, Phys. Plasmas 7, 3017 (2000).

[56] K. Schmid, A. Buck, C. M. S. Sears, J. M. Mikhailova, R. Tautz, D. Herrmann, M. Geissler, F. Krausz, and L. Veisz, Density-transition based electron injector for laser driven wakefield accelerators, Phys. Rev. ST Accel. Beams 13, 091301 (2010).

[57] A. Buck, J. Wenz, J. Xu, K. Khrennikov, K. Schmid, M. Heigoldt, J. M. Mikhailova, M. Geissler, B. Shen, F. Krausz, S. Karsch, and L. Veisz, Shock-front injector for high-quality laser-plasma acceleration, Phys. Rev. Lett. 110, 185006 (2013).

[58] S. Chou, J. Xu, K. Khrennikov, D. E. Cardenas, J. Wenz, M. Heigoldt, L. Hofmann, L. Veisz, and S. Karsch, Collective deceleration of laser-driven electron bunches, Phys. Rev. Lett. 117, 144801 (2016).

[59] See Supplemental Material at http://link.aps.org/supplemental/10.1103/PhysRevLett.132.045001 for the electron injection in the laser-modulated wakefield, the temporal evolution of the spin precession frequency, the parametrization of the sharp downward density jump, and the production of the electronic polarized gas target.

[60] H. M. Mott-Smith, The solution of the Boltzmann equation for a shock wave, Phys. Rev. 82, 885 (1951).

[61] J. Vieira and J. T. Mendonça, Nonlinear laser driven donut wakefields for positron and electron acceleration, Phys. Rev. Lett. 112, 215001 (2014).

[62] J. Thomas, A. Hützen, A. Lehrach, A. Pukhov, L. Ji, Y. Wu, X. Geng, and M. Büscher, Scaling laws for the depolarization time of relativistic particle beams in strong fields, Phys. Rev. Accel. Beams **23**, 064401 (2020).

[63] S. R. Mane, Y. M. Shatunov, and K. Yokoya, Spin-polarized charged particle beams in high-energy accelerators, Rep. Prog. Phys. **68**, 1997 (2005).

[64] T. D. Arber, K. Bennett, C. S. Brady, A. Lawrence-Douglas, M. G. Ramsay, N. J. Sircombe, P. Gillies, R. G. Evans, H. Schmitz, A. R. Bell, and C. P. Ridgers, Contemporary particle-in-cell approach to laser-plasma modelling, Plasma Phys. Controlled Fusion **57**, 113001 (2015).

[65] F. Wan, W.-Q. Wang, Q. Zhao, H. Zhang, T.-P. Yu, W.-M. Wang, W.-C. Yan, Y.-T. Zhao, K. Z. Hatsagortsyan, C. H. Keitel, S. V. Bulanov, and J.-X. Li, Quasimonoenergetic proton acceleration via quantum radiative compression, Phys. Rev. Appl. **17**, 024049 (2022).

[66] S. Carbajo, E. Granados, D. Schimpf, A. Sell, K.-H. Hong, J. Moses, and F. X. Kaertner, Efficient generation of ultra-intense few-cycle radially polarized laser pulses, Opt. Lett. **39**, 2487 (2014).

[67] F. Kong, H. Larocque, E. Karimi, P. B. Corkum, and C. Zhang, Generating few-cycle radially polarized pulses, Optica **6**, 160 (2019).

[68] H. Zhong, C. Liang, S. Dai, J. Huang, S. Hu, C. Xu, and L. Qian, Polarization-insensitive, high-gain parametric amplification of radially polarized femtosecond pulses, Optica **8**, 62 (2021).